Polymer–Organoclay Hybrids by Polymerization into Montmorillonite-Vinyl Monomer Interlayers

Ahmed Rehab, Ahmed Akelah, Tarek Agag, Mohamed Betiha

Chemistry Department, Faculty of Science, University of Tanta, 31527 Tanta, Egypt

Received 30 August 2006; accepted 8 February 2007
DOI 10.1002/app.26335
Published online 27 August 2007 in Wiley InterScience (www.interscience.wiley.com).

ABSTRACT: A different series of polymer–clay hybrid materials have been prepared by modification of the clay with different vinyl monomers, followed by polymerization of different ratios of vinyl monomers–clay with the monomers, such as methyl methacrylate, hydroxyethyl methacrylate, and styrene-maleic anhydride. The materials were investigated by IR, which confirmed the intercalation of vinyl-cation within the clay interlayers, and by TGA, which illustrated that phosphonium cation has high thermal stability than ammonium cation. Swelling studies of these materials in different organic solvents showed that the swelling degree increases as clay ratio decrease, and also showed higher swelling relative to vinyl–clay. X-ray diffraction illustrated that the nanocomposites were exfoliated up to a 25 wt % content of organoclay relative to the amount of polymer. SEM and TEM examined the micrograph, which showed a good dispersion of the polymers into clay galleries, and formation of nanosize particles ranged 150–300 Å. © 2007 Wiley Periodicals, Inc. J Appl Polym Sci 106: 3502–3514, 2007

Key words: polymer–clay hybrids; nanocomposite materials; PMMA-nanocomposites; organic–inorganic composites

INTRODUCTION

The commercial importance of polymeric composites has received considerable interest in various application fields, such as aerospace, automotive, marine, infrastructure, military, etc.[1] It has been found that silicate-filled polymer composites often exhibit remarkable improvement of mechanical, thermal, and physicochemical properties when compared with pure polymers. Their microcomposites have great attention because of the nano-level interactions of the silicate layers with the polymer matrix and their low cost, abundance, and high aspect ratio that give greater possibility of energy transfer from one phase to another.[1–3]

In layered clay-polymer composites with nanometer dimensions, the interfacial effect between the silicate layers and polymer matrix and the completely homogenized dispersion of the silicate layers in the polymer matrix are the factors leading to improved properties.[4] However, it is extremely difficult to achieve complete exfoliation of the layers due to the strong electrostatic interactions between silicate layers and intragallery cations. A successful attempt to avoid this difficulty is carried by replacing such inorganic cations by some quarternized ammonium or phosphonium salts, preferably with long alkyl chain, i.e., lipophilization of the clays.[5] Such alkylammonium or alkylphosphonium cations reduce the surface polarity (hydrophilic) of the silicate layers and enhance the affinity between the silicate and the polymer matrix.[4,6] In polymer–clay nanocomposites the movement of the polymer chains is confined, and then the interactions among the polymer chains are greatly affected by the confinement of the nanometer space. Generally, the polymer–clay nanocomposites have been prepared by four techniques: polymer-adsorption,[7,8] *in situ* intercalative polymerization,[9,10] melt intercalation,[11,12] and template synthesis.[13]

From the structural point of view, two types of polymer-layered silicate structures are possible: intercalated and exfoliated ones. In exfoliated nanocomposites, the silicate layers of montmorillonite (MMT) are completely separated into individual nanometer thick (about 1 nm) layers and uniformly dispersed in the continuous polymer matrix. In the intercalated nanocomposites, a single (and sometimes more than one) extended polymer chain is intercalated between the silicate layers, resulting in a well-ordered multiplayer morphology built up with alternating polymeric and silicate layers. In reality, instead of ideal exfoliated or intercalated nanocomposites, it is more common to obtain partially exfoliated and partially intercalated nanocomposites, in which silicate layers of MMT are exfoliated into nanometer secondary particles (several silicate layers stacked against each other) and uniformly dispersed in the polymer matrix. Moreover, these systems may still exhibit substantial improvement of their physical properties.

Some studies have been reported for PMMA-MMT nanocomposites, which include the different preparation methods, the structure, and improved properties

Correspondence to: A. Rehab (rehab220956@yahoo.com).

Journal of Applied Polymer Science, Vol. 106, 3502–3514 (2007)

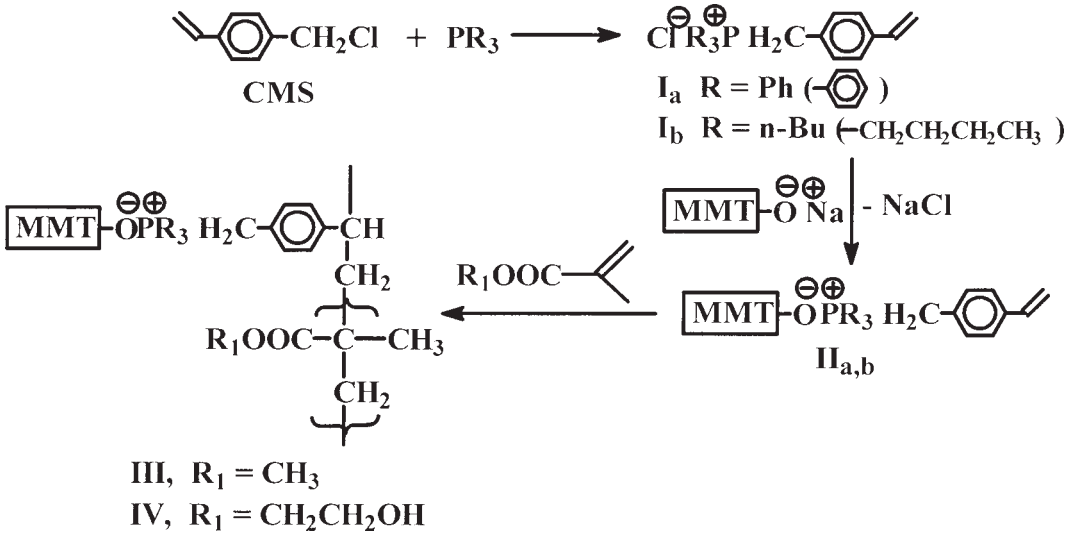

Scheme 1 Preparation of triphenyl and tributyl (4-vinylbenzyl) phosphonium salt–clay and its polymerization with MMA and HEMA.

of the final hybrid.[14–17] In continuous of this work for the synthesis of polymer–clay hybrids, which can exhibit the characteristic properties of the individual components, the present study includes the polymerizations of the methyl methacrylate, hydroxyethyl methacrylate, and styrene-maleic anhydride with different ratios of vinyl monomer–clay by *in situ* free-radical polymerization technique.

EXPERIMENTAL

Materials

Pristine sodium montmorillonite clay (Na^{+}-O-MMT), trade name Kunipia-F, with cation exchange capacity of ~ 119 mequiv per 100 g, and *n*-octadecylamine and *N,N*-dimethyl-*n*-octadecylamine were supplied by Kunimine Industry (Japan).

Chloromethylstyrene (CMS) (vinylbenzyl chloride) was obtained from Polyscience (Eppelheim, Germany), as a mixture of m-/*p*-isomers (≈ 30/60%) and used as supplied.

Methylmethacrylate (MMA) and styrene (St) were supplied from Aldrich (Graz, Austria) and used after discharge the inhibitor by washing with 1*M* NaOH solution, then dried over Na_2SO_4, which was used as purchased from Aldrich, without further purification.

2-Hydroxyethyl-methacrylate (HEMA), triphenylphosphine, tributylphosphine, and 2,2-azobisisobutyronitrile (AIBN) were obtained from Fluka (Switzerland) and used without further purification.

Maleic anhydride (MA) was used as supplied from Merck-Schuchardt (Germany).

Benzoyl peroxide (BPO) was used as supplied from BDH Laboratory Reagents, Chemical (England).

Dimethylformamide (DMF) and toluene were obtained from Adwic (Egypt) and used after distillation and drying over A4 molecular sieve directly. Ethanol, methanol, and diethyl ether were used as obtained from Adwic, without further purification.

Preparation of salt of vinyl monomers ($I_{a–d}$)

Generally, the vinyl monomers $I_{a–d}$ were prepared according to the procedure described previously[18] and illustrated in Schemes 1 and 2.

Synthesis of triphenyl-(4-vinylbenzyl) phosphonium chloride salt, I_a

The vinyl monomer salt I_a was prepared by mixing of a solution of 10.49 g (40 mmol) triphenylphosphine dissolved in 60 mL of dry DMF with 6.11 g (40 mmol) vinylbenzyl chloride in presence of 0.03 g of hydroquinone as free-radical inhibitor. The yield of the recrystallized product was found 13.12 g (87% yields) of triphenyl-(4-vinylbenzyl) phosphonium chloride I_a. The structure was confirmed by nuclear magnetic resonance (NMR) and infrared (IR) spectroscopic methods and the data was corresponding with Ref. 18.

Synthesis of tributyl-(4-vinylbenzyl) phosphonium chloride salt, I_b

Preparation of this compound was carried out by dissolving a mixture of 4 g (26.2 mmol) of vinylbenzyl chloride, 5.31 g (26 mmol) of tributylphosphine, and 0.02 g of hydroquinone in 50 mL dry DMF, followed by stirring at room temperature. The procedure was completed as previously described[18] to give 8.15 g of the salt I_b, which corresponds to 87% of the product yield. The characterization of I_b was carried out by

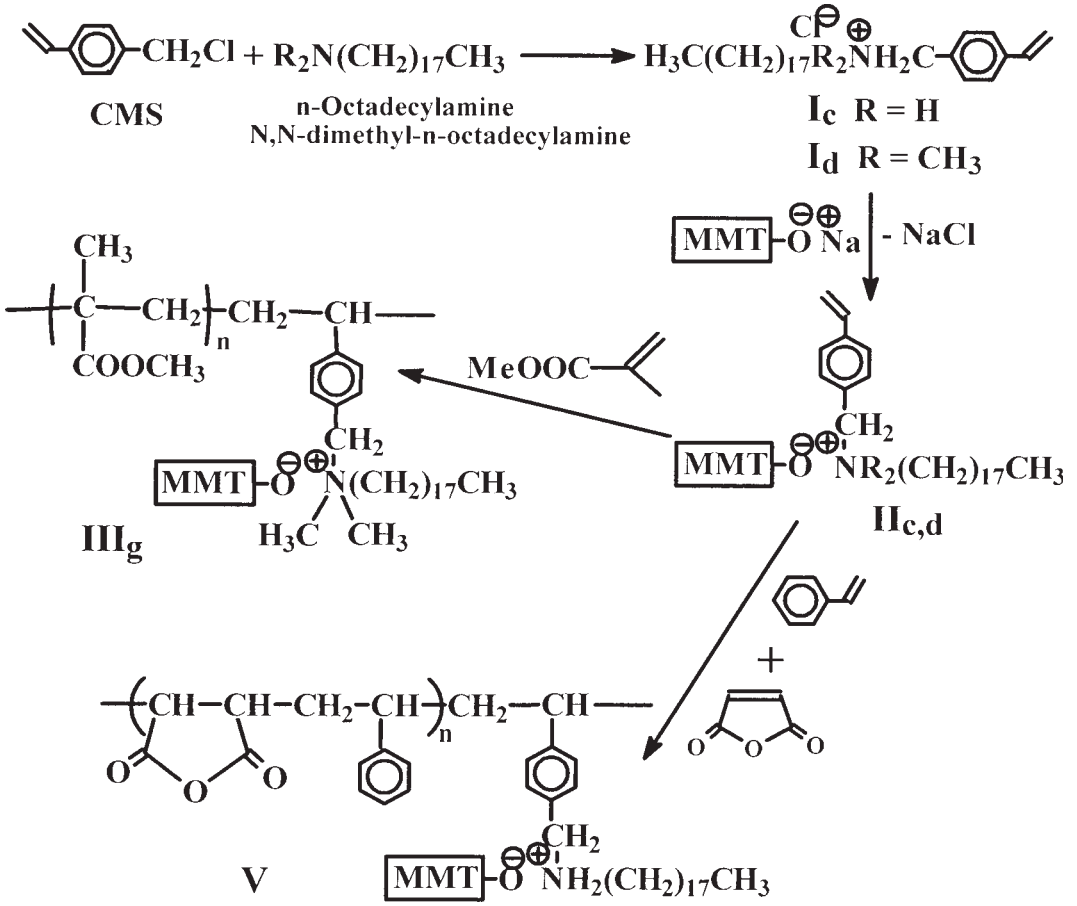

Scheme 2 Preparation of octadecyl (4-vinylbenzyl) ammonium salt–clay, *N,N*-dimethyl-*n*-octadecyl (4-vinylbenzyl) ammonium salt–clay, and its polymerization with MMA and styrene-*co*-maleic anhydride.

NMR and IR spectroscopic analysis and the data was corresponding with Ref. 18.

Synthesis of n-octadecyl-(4-vinylbenzyl) ammonium chloride salt, $\mathbf{I_c}$

To the stirred solution mixture of 10.78 g (40 mmol) stearylamine and 0.03 g of hydroquinone dissolved in 50 mL of dry DMF at 45°C, 6.1 g (40 mmol) of vinylbenzyl chloride was added dropwise in a period 4 h. The precipitated product was filtered and washed with diethyl ether, and then dried in vacuum at room temperature to give 13.84 g of salt $\mathbf{I_c}$ with 82% product yield. The characterization of $\mathbf{I_c}$ was carried out by NMR and IR spectroscopic analysis and the data was corresponding with Ref. 18.

Synthesis of N,N-dimethyl-n-octadecyl-(4-vinylbenzyl) ammonium chloride salt, $\mathbf{I_d}$

A mixture of 10.41 g (35 mmol) of *N,N*-dimethyl-*n*-octadecylamine dissolved in 10 mL of dry THF and 5.34 g (35 mmol) of vinylbenzyl chloride was stirred for 2 h at room temperature. An excess of diethyl ether was added and the mixture was stirred for 2 h. The precipitated product was filtered off, and recrystallized from ethyl acetate at 45°C, to give 14.36 g of $\mathbf{I_d}$ (yield = 91%). The characteristic data was corresponding to data in reference.[18]

Preparation of vinyl monomer–clay $\mathbf{II_{a–d}}$

General procedure

The formation of intercalated vinyl monomers into clay interlayer was followed the preparation of $\mathbf{II_a}$, procedure previously described in our work.[18]

It was achieved by dropwise addition with stirring of a solution of 4.93 g (11.9 mmol) of $\mathbf{I_a}$ dissolved in 100 mL of distilled water to a swelled 10 g (11.9 mequiv) of sodium montmorillonite in 300 mL of distilled water and 30 mL of ethanol. The dry white powder product was 12.85 g of $\mathbf{II_a}$.

XRD data: $2\theta = 3.82^\circ$; *d*-spacing = 23.12 Å.

Calcination data: Inorganic contents = 77.4 (wt %); organic contents = 22.6 (wt %).

The vinyl monomer–clay $\mathbf{II_b}$ was prepared by the same procedure by the addition of 4.22 g (11.9 mmol) $\mathbf{I_b}$ dissolved in 100 mL of distilled water to a stirred 10 g of swelled clay to produce 12.2 g of $\mathbf{II_b}$.

TABLE I
Preparation Condition Data for PMMA-Clay and PHEMA-Clay Composite Materials

	Organoclay		Monomer		Solvent		Product		
								Ungrafted[b]	
Run	Type	Wt (g)	Type	Wt (g)	Type	Volume (mL)	Grafted[a] (g)	Wt (g)	(η_{rel})
$\mathbf{III_a}$	$\mathbf{II_a}$	0.1	MMA	9.9	Tol	10	0.2712	7.1137	1.2301
$\mathbf{III_b}$	$\mathbf{II_a}$	0.5	MMA	9.5	Tol	15	0.8646	3.9559	1.1524
$\mathbf{III_c}$	$\mathbf{II_a}$	1.0	MMA	9.0	Tol	30	1.7381	3.6237	1.1810
$\mathbf{III_d}$	$\mathbf{II_a}$	2.5	MMA	7.5	Tol	75	3.7634	0.9786	1.2190
$\mathbf{III_e}$	$\mathbf{II_c}$	0.5	MMA	9.5	–	–	1.002	8.4123	1.2190
$\mathbf{III_f}$	$\mathbf{II_c}$	1.0	MMA	9.0	–	–	3.3458	5.5079	1.2857
$\mathbf{III_g}$	$\mathbf{II_d}$	4.0	MMA	6.0	Tol	70	8.5		–
$\mathbf{IV_a}$	$\mathbf{II_c}$	0.1	HEMA	9.9	Diox	2.5	9.6182	0.3801	1.2381
$\mathbf{IV_b}$	$\mathbf{II_c}$	0.5	HEMA	9.5	Diox	–	2.6927	3.9215	1.3429
$\mathbf{IV_c}$	$\mathbf{II_c}$	1.0	HEMA	9.0	Diox	5	4.0	1.818	1.8190
$\mathbf{IV_d}$	$\mathbf{II_c}$	2.5	HEMA	7.5	Diox	10	3.1984	1.4306	1.2952

[a] The insoluble product obtained after washing with Soxhlet.
[b] The soluble product in toluene on washing with Soxhlet.

XRD data: 2θ = 4.83°; *d*-spacing = 18.29 Å.

Calcination data: Inorganic contents = 69.7 (wt %); organic contents = 30.3 (wt %).

The ammonium salt of Vinyl monomer–clay $\mathbf{II_c}$ was prepared by carrying the same procedure used in the preparation of $\mathbf{II_a}$, by dropwise addition of 5 g (11.9 mmol) ammonium salts $\mathbf{I_c}$ dissolved in 100 mL of water/methanol (70:30, v/v) to a stirred 10 g of swelled clay, followed by stirring for 8 h to give 12.8 g of $\mathbf{II_c}$.

XRD data: 2θ = 3.83° and 7.1°; *d*-spacing = 23 and 12.4 Å.

Calcination data: Inorganic contents = 66.6 (wt %); organic contents = 33.4 (wt %).

The synthesis of vinyl monomer–clay $\mathbf{II_d}$ was carried out by dropwise addition of 5.36 g (11.9 mmol) ammonium salts $\mathbf{I_d}$ dissolved in 100 mL of water/methanol [70 : 30 V/V] to 10 g of swelled clay followed by stirring for 8 h to give 13.9 g of $\mathbf{II_d}$.

XRD data: 2θ = 2.63° and 4.78° and 7.2°; *d*-spacing = 33.6 and 18.48 and 12.4.

Calcination data: Inorganic contents = 50.76 (wt %); organic contents = 49.24 (wt %).

Preparation of polymer–organoclay nanocomposites III, IV, and V

Preparation of PMMA–organoclay composites $\mathbf{III_{a–f}}$

General procedure. Synthesis of $\mathbf{III_d}$: A mixture of 2.5 g organoclay $\mathbf{II_a}$ swelled in 75 mL of dry toluene, 7.5 g of MMA monomer, and 0.1 g of AIBN as a radical initiator was stirred at room temperature for about 5 h until a homogenous (well swelled) suspension was obtained. The mixture was heated at ~ 80°C for 2 h, and after cooling, the suspended product was precipitated in an excess of methanol with stirring. After stirring for a few hours, the precipitated PMMA-MMT product was filtered, washed several times with methanol, and finally dried under vacuum at 60°C for 24 h to give 3.75 g of composite $\mathbf{III_d}$.

The data relevant of the other composite samples with different ratios of organoclay with and without solvent were prepared by following the same procedure as summarized in Table I.

Preparation of PHEMA–clay nanocomposites $\mathbf{IV_{a–d}}$

A mixture of 1.0 g modified clay $\mathbf{II_c}$, 0.1 g AIBN dissolved in 5 mL 1,4-dioxane, and 9.0 g of HEMA monomer was stirred at room temperature for about 5 h to give a homogeneous suspension, and then heated at ~ 80°C for 2 h. After cooling, the product was poured on an excess of methanol and stirred overnight. The white precipitated polymer–MMT was filtered off, washed with methanol, and dried in vacuum at 60°C to give 5.9 g of the PHEMA–clay nanocomposite $\mathbf{IV_c}$. The other samples $\mathbf{IV_{a–d}}$ were prepared by the same procedure with different ratios (1,5, 10, and 25 wt %) of the same organoclay as shown in Table I.

Preparation of P(St-co-MA)–clay nanocomposites $\mathbf{V_{a–h}}$

To a mixture of 4.633 g, 44.5 mmol St, 4.36 g, 44.5 mmol MA, and 0.1 g of BPO as a radical initiator dissolved in 20 mL dry toluene, 1 g of organoclay $\mathbf{II_b}$ was added. The mixture was stirred at room temperature for about 5 h until a homogeneous suspension was obtained, and then heated at about 80°C for 2 h. After cooling, the product was precipitated by addition the colloidal suspension to an excess of methanol. The precipitated polymer–MMT hybrid was filtered, washed with methanol, and dried in vacuum at 60°C to give 9.5 g of P(St-*co*-MA)–clay nanocomposite. The other samples were prepared by the same procedure using different ratios of organoclay (1, 5, 10, and 25%) and different solvents (acetonitrile, 1,4-dioxane), as illustrated in Table II.

TABLE II
Preparation Condition Data for P(St-*co*-MA)-Clay Composite Materials

	Organoclay		Monomer		Solvent		Product		
								Ungrafted[b]	
Run	Type	Wt (g)	St (g)	MA (g)	Type	Volume (mL)	Grafted[a] (g)	Wt (g)	(η_{rel})
$\mathbf{V_a}$	$\mathbf{II_b}$	0.1	5.096	4.802	Tol	5	0.2093	9.2201	1.3905
$\mathbf{V_b}$	$\mathbf{II_b}$	0.5	4.89	4.60	Tol	10	0.8584	8.212	1.1810
$\mathbf{V_c}$	$\mathbf{II_b}$	0.5	4.89	4.60	MeCN	5	1.1842	7.8722	1.2571
$\mathbf{V_d}$	$\mathbf{II_b}$	1.0	4.633	4.36	Tol	20	1.5001	8.0135	1.1524
$\mathbf{V_e}$	$\mathbf{II_b}$	1.0	4.633	4.36	MeCN	8	1.6684	6.6684	1.2190
$\mathbf{V_f}$	$\mathbf{II_b}$	2.5	3.86	3.64	Tol	45	3.3958	1.669	1.1429
$\mathbf{V_g}$	$\mathbf{II_c}$	0.5	4.89	4.60	Diox	5	0.7045	5.5429	1.2095
$\mathbf{V_h}$	$\mathbf{II_c}$	1.0	4.633	4.36	Diox	10	2.263	1.9673	1.2286

[a] The insoluble product obtained after washing with Soxhlet.
[b] The soluble product in toluene on washing with Soxhlet.

Analytical procedures

^1H and ^{13}C NMR spectroscopic measurements were recorded in $CDCl_3$ with an Iambda Jeol NM300 spectrometer (Fig. 1).

IR spectra were carried out on a Perkin–Elmer 1430 ratio-recording infrared spectrophotometer using the potassium bromide disc technique in the wave number range of 4000 to 200 cm^{-1}, Figure 2.

The swelling degree was determined by taking a definite weight (about 0.15 g) of the dry sample and introduced into a small sintered glass and allowed to imbibe in different solvents for 24 h. The excess solvent was removed by gentle centrifugation. The swelled sample was weighed and resuspended in the solvent. This procedure was repeated until obtaining a constant weight for the swelled sample. The swelling degree of each sample is expressed as the amount of sorbed solvent per 100 g of dry sample, as summarized in Table III.

Thermogravimetric analyses (TGA) were determined with Rigaku Thermo Plus 2 TG-DTA TG8120. The heating rate was 5–10°C min^{-1} under air and argon atmosphere in the temperature range ~ 30–900°C (Table IV, Figs. 3 and 4).

X-ray diffraction (XRD) measurements were carried out using a Phillips Powder-Diffractometer equipped with a Ni-filtered Cu K radiation ($\lambda = 1.5418$ Å) at scanning rate of 0.005°/s, diverget slit 0.3°. Measurements were made for the dried product to examine the interlayer activity in the composite as prepared (Figs. 5–8).

Calcinations measurements: A definite weight of the sample was introduced into a porcelain crucible and dried in an electric oven at 120°C overnight, then introduced into an ignition oven, and the temperature was increased to 1000°C and adjusted at this temperature for 5 h. The loading of each sample expressed as the weight loss by ignition per 100 g of the dry sample.

Morphology of the composite was examined by a Joel JXA-840 scanning electron microscopy (SEM) equipped with an energy dispersive X-ray detector to examine the morphology and particle size of MMT in the polymer–MMT composites. Specimen was deposited on double-sided scotch tape and examined at their surface (Figs. 9–11).

Transmission electron microscopy (TEM) images of the composites were obtained by a Joel 100 CX at 80 kV. The microstructure of PMMA and PSMA/organoclay mixtures were examined in TEM. The specimens were prepared at room temperature in thin film using diamond knife. The sections (nominal thickness of 70 nm) were transferred from water to 200-mesh Cu grids. The microtome surface was observed as shown in Figures 12 and 13.

RESULTS AND DISCUSSION

MMT clay is a smectite-layered aluminosilicate in which each plate-like layer is about 1.0 nm thick and 50–100 nm in lateral dimension. The surfaces of the layer are mainly made up of silica tetrahedral, whereas the central plane of the layer contains octrahedrally coordinated Al^{3+} with frequent nonstoichiometric substitutions, where Al^{3+} ions are replaced by Mg^{2+} and sometimes by Fe^{3+}. Mg^{2+} ions substitution leaves an embedded negative charge in the clay, which must be neutralized with a cation at the surface, usually Na^+ ions.

To prepare polymer–clay nanocomposites, the gallery space must be large and sufficiently organophobic to permit the entry of the organic polymer. The usual treatment is to replace the inorganic ions of clay by ammonium or phosphonium ions that contain at least one long alkyl chain or many aromatic rings. The identity of the cation can be critical to the formation of the nanocomposite. The method of preparation to be used affects also the choice of the organically modified clay.

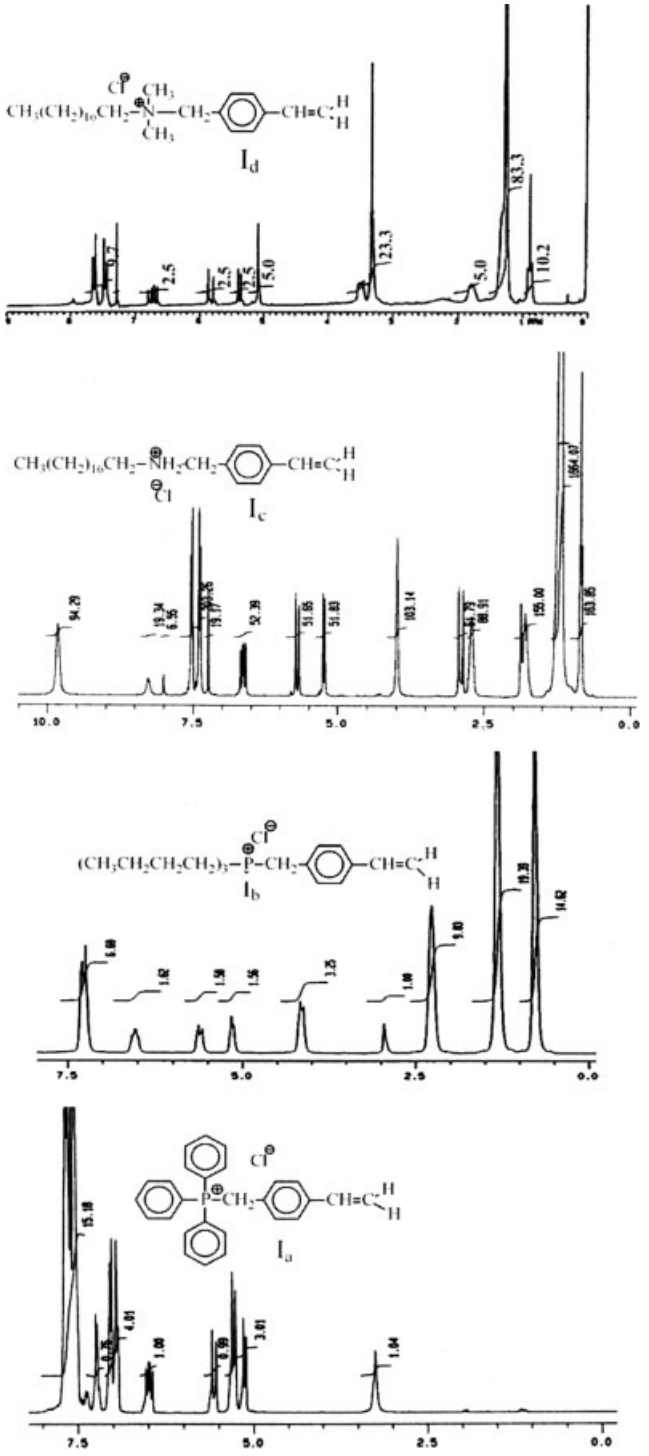

Figure 1 H^1 NMR spectra the monomers $\mathbf{I_{a–d}}$.

The preparation of the polymer–clay composites was carried out through several steps as illustrated in Schemes 1 and 2. The first step includes the formation of monomeric salts such as triphenyl-(4-vinylbenzyl)-phosphonium chloride salt $\mathbf{I_a}$, tributyl-(4-vinylbenzyl)phosphonium chloride salt $\mathbf{I_b}$, octadecyl-(4-vinylbenzyl)ammonium chloride salt $\mathbf{I_c}$, and *N,N*-dimethyl-*n*-octadecyl-(4-vinylbenzyl)ammonium chloride salt $\mathbf{I_d}$. The second step includes the preparation of vinyl monomer–clay intercalates. This step was achieved by cation exchange between onium groups of vinyl monomer and Na-cations presented in the clay surface and in the interlayers to form ionic bond with MMT clay. The final step includes the dispersion of different ratios (1, 5, 10, 25, 40 wt %) of vinyl monomer–clay in the monomer by complete swelling, followed by solution or bulk free-radical polymerization to produce the polymer–clay exfoliated and intercalated nanocomposites. The relevant polymerization condition data for the different series of polymers–clay nanocomposite materials are summarized in Tables I and II. The data in the tables show that there are many factors affecting the amount of grafted polymer onto clay in the composite products, such as amounts of vinyl-MMT type, solvent type, and monomer type. The amount of grafted polymers was determined by extraction process in toluene, DMF, or acetone using soxhlet system, and the soluble part gives the ungrafted products. The data in the Tables I and II show that the amount of grafted polymers decreases with increasing the ratio of vinyl monomer-MMT. This may be due to chain transfer termination caused by MMT[19] and isothermal property of MMT,[18] which prevent the complete polymerization process.

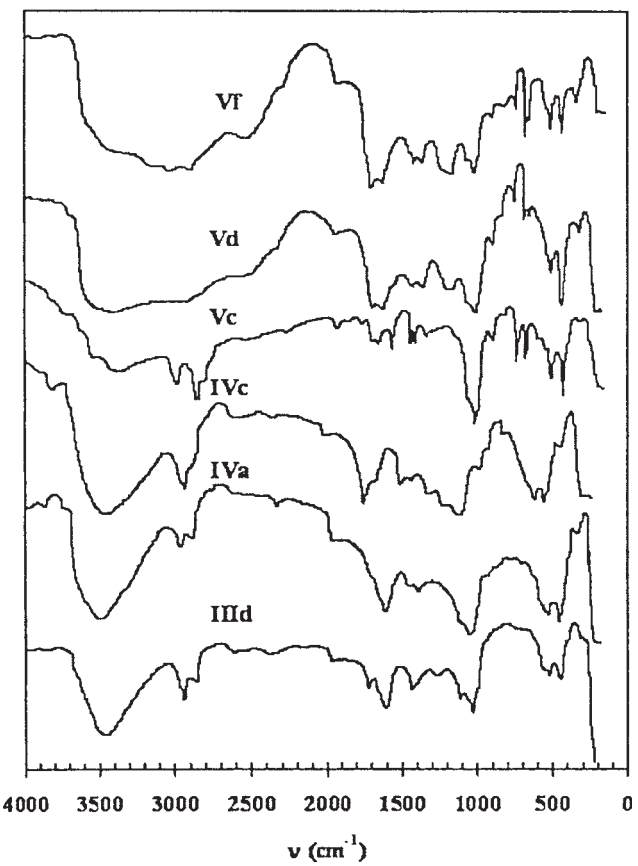

Figure 2 IR spectra for PMMA–organoclay $\mathbf{III_d}$, PHEMA–organoclay $\mathbf{IV_{a,c}}$, and P(St-*co*-MA) $\mathbf{V_{c,d,f}}$ nanocomposites.

TABLE III
Swelling Data for the Monomer-Clay and Grafted Polymer-Clay Composites

	Swelling data						
Run	DMF	Acetone	Toluene	CH_3Cl	CH_2Cl_2	Dioxan	H_2O
$\mathbf{II_a}$	1158	394	190	219	312	190	–
$\mathbf{II_b}$	955	224	701	228	226	155	–
$\mathbf{II_c}$	365	250	143	262	152	187	–
$\mathbf{III_a}$	1486	620	687	755	1150	855	184
$\mathbf{III_b}$	1360	602	634	481	1047	475	280
$\mathbf{III_c}$	1783	534	661	414	1024	423	210
$\mathbf{III_d}$	1090	524	601	361	592	203	280
$\mathbf{III_e}$	359	65	373	286	11	297	15
$\mathbf{III_f}$	115	24	87	200	37	50	101
$\mathbf{III_g}$	–	–	–	–	–	–	–
$\mathbf{IV_a}$	1131	29	88	23	22	168	48
$\mathbf{IV_b}$	550	44	97	36	36	185	103
$\mathbf{IV_c}$	734	18	15	42	34	148	192
$\mathbf{IV_d}$	144	7	41	11	16	49	86
$\mathbf{V_a}$	971	223	541	95	931	225	358
$\mathbf{V_b}$	537	180	336	60	161	213	100
$\mathbf{V_c}$	600	220	237	210	670	810	50
$\mathbf{V_d}$	496	123	270	40	25	185	179
$\mathbf{V_e}$	407	150	210	192	659	759	37
$\mathbf{V_f}$	496	123	206	30	21	147	156
$\mathbf{V_g}$	395	65	86	38	39	129	6
$\mathbf{V_h}$	115	24	87	200	37	150	20

DMF, acetone, toluene, CH_3Cl, CH_2Cl_2, dioxin, and H_2O are the solvents used.

The vinyl monomer-MMT type affects the amount of polymer grafted onto clay interlayers; samples $\mathbf{III_{e,f}}$ give high grafted polymer on using vinyl monomer-MMT $\mathbf{II_c}$ than the samples $\mathbf{III_{b,c}}$ on using vinyl monomer-MMT $\mathbf{II_a}$. This can be illustrated by the presence of hydrogen bond between carbonyl groups of MMA and both oxygen group of silicate and $—N^+H_2—$ of vinyl surfactant.[20]

The monomer type shows an effective factor on the grafting polymerization onto the surfaces and interlayers of the clay and is found in the order HEMA > St/MA > MMA. This can be related to the chemical structure of monomers; since HEMA has two different functional groups (carbonyl and hydroxyl groups), St/MA has two similar functional groups (carbonyl groups) and MMA have one carbonyl group, which led to anchor the clay layers with monomers, due to the strong hydrogen-bonding interactions in the previous order.[20] This may explain why higher hydrogen bonds play an important role in the swelling and exfoliation of clay layers. However, exothermic reaction of St-MA overcomes the isothermal character of clay, which led to increasing the grafted polymer onto clay.

The solvent used plays pronounced effect on the formation of polymer–clay composites. The data in Tables I and II illustrate that the use of acetonitrile as good swellable solvent for $\mathbf{II_b}$ leads to an increase the grafted polymers in samples $\mathbf{V_{c,e}}$ than in the case of using toluene as in the samples $\mathbf{V_{b,d}}$. This can be illustrated by increasing the rate of penetration of the monomer inside clay galleries that leads to increased grafting. This significant penetration of monomer is attributed to the high dipole moment of MeCN, which

TABLE IV
Thermal Analysis Data for the Monomer-Clay and Some Grafted Polymer-Clay Composites

	TGA data							Calcination	
				TDR					
Run	$cT_{0.05}$	$T_{0.1}$	$T_{0.5}$	Start	End	Wt loss (%)	Char (%)	Org. (%)	Inorg. (%)
$\mathbf{II_a}$	381	424	–	315	511	18	82	29.6	70.4
$\mathbf{II_c}$	265	371	–	100	461	28	72	44.4	56.6
$\mathbf{II_d}$	248	267	–	221	433	22	55	49.2	50.8
				433	641	19			
				641	733	4			
$\mathbf{III_b}$	340	376	–	256	511	33	61	69.0	31.0
				456	664	6			
$\mathbf{III_c}$	320	358	–	272	480	40	55	71.0	29.0
				534	625	5			
$\mathbf{III_g}$	246	361	350	220	307	34	16	80.0	20.0
				307	433	38			
				407	617	12			
$\mathbf{IV_b}$	232	287	406	191	257	8	12	86.0	14.0
				296	339	28			
				389	464	52			
$\mathbf{V_b}$	171	263	–	120	336	15	68	–	–
				345	354	17			
$\mathbf{V_d}$	362	406	–	288	620	21	79	–	–
$\mathbf{V_e}$	248	300	410	171	505	59	41	–	–
$\mathbf{V_h}$	122	147	374	100	265	41	37	–	–
				265	380	10			
				380	460	12			

TDR, temperature decomposition range.

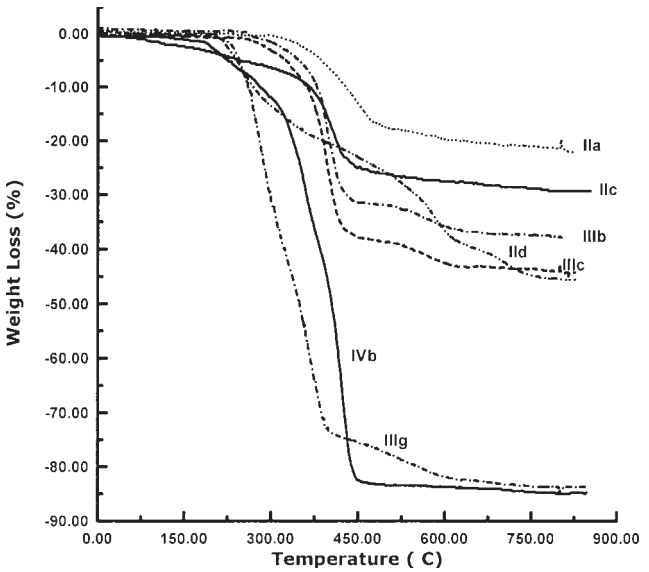

Figure 3 TGA thermograms for vinyl–clay, PMMA–organoclay, and PHEMA–organoclay composites.

appears to have caused the association in the liquid state.[19] In another way, the acetonitrile is a good solvent for St and MA monomers, but it is a poor solvent for PSMA, which leads to increase in gellation and the conversion of monomers to polymers increases than in toluene. This supported the idea that the organoclay $\mathbf{II_b}$ have been delaminated in the St-MA monomer and the poor solubility of PSMA in MeCN prevents reforming aggregation.

The bulk polymerization for MMA into vinyl monomer–clay interlayers leads to a highly dispersed clay into polymer matrix. For example, in the samples $\mathbf{III_e}$ and $\mathbf{III_f}$, the organoclay $\mathbf{II_c}$ are highly swelled in

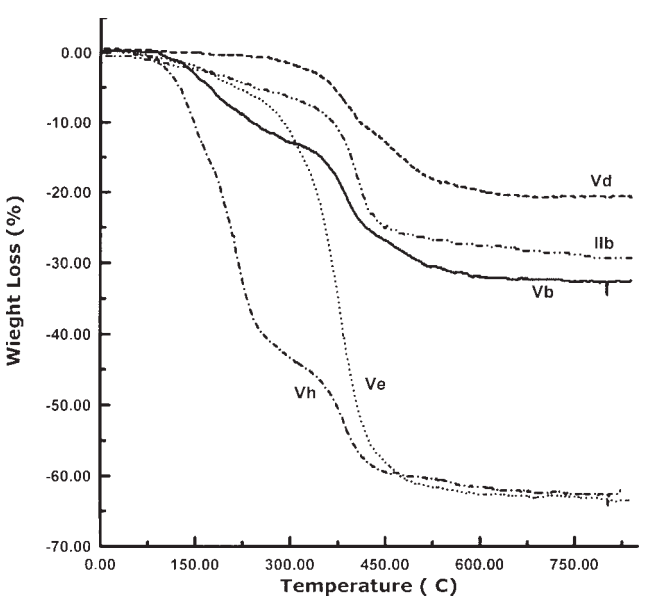

Figure 4 TGA thermograms of vinyl monomer–clay $\mathbf{II_b}$ and some samples of P(St-*co*-MA)–clay $\mathbf{V_{a–h}}$.

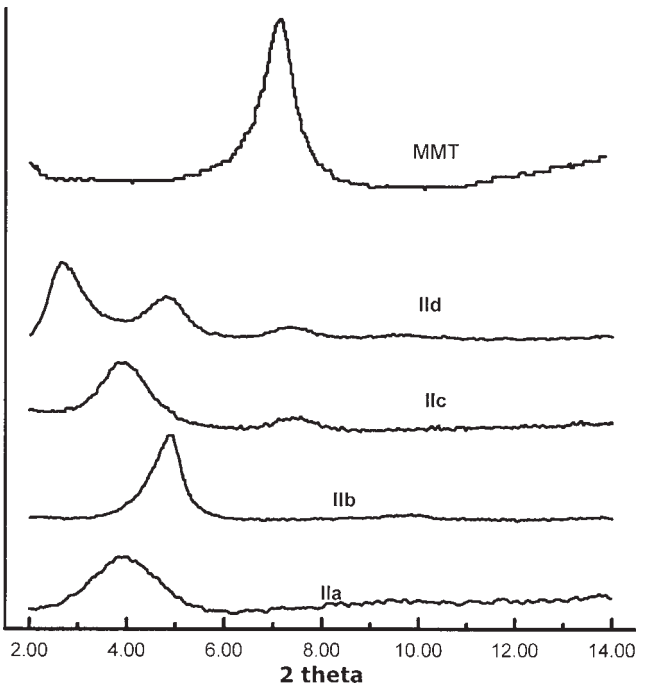

Figure 5 XRD for MMT clay and vinyl monomer–clay intercalates $\mathbf{II_{a–d}}$.

MMA monomer without solvent, followed by bulk free-radical polymerization, to give product, a highly suspended (semiclear) solution in toluene. A possible reason is the high polymerization rate for PMMA, due to the high rate of propagation and the pronounced gel effect. The gel effect is most important because it causes a sharp decrease in the termination rate and leads to an increase in the overall polymerization rate and in molecular weight.[21]

The structural composition of vinyl monomer salts were identified by ^{1}H NMR, ^{13}C NMR, and IR spectroscopy. The ^{1}H NMR data (Fig. 1) were recorded for vinyl monomers $\mathbf{I_{a–d}}$ in the experimental part, in which the H of chloromethyl group (CH_2Cl) was shifted from 4.6 ppm for CMS to 5.3 ppm corresponding to the quaternary salt for $\mathbf{I_a}$, to 4.17 ppm for $\mathbf{I_b}$, to 3.98 ppm for $\mathbf{I_c}$, and to 4.2 ppm for $\mathbf{I_d}$. The peak at about 6 ppm corresponding to amine proton of stearylamine (Fig. 1) disappeared and a new peak appeared at 9.8 ppm with integration of two protons corresponding to $—^+NH_2—$. Also, the peaks at 5.0, 5.6, and 6.6 ppm revealed the presence of vinyl group. ^{13}C NMR spectra show absorption band at 46 ppm corresponding to one carbon of chloromethyl group (CH_2Cl), which was shifted to 30 ppm corresponding to the quaternary salt for $\mathbf{I_a}$, to 26 ppm for $\mathbf{I_b}$, and to 29 ppm for $\mathbf{I_c}$.

The IR spectra of vinyl monomers showed an absorption band at 717 cm^{-1} for chloromethyl group, which disappeared in the intercalated vinyl monomers $\mathbf{II_{a–c}}$. Also, a characteristic band related to vinyl group (—C=C—) was found at 1614 cm^{-1} for $\mathbf{I_a}$,

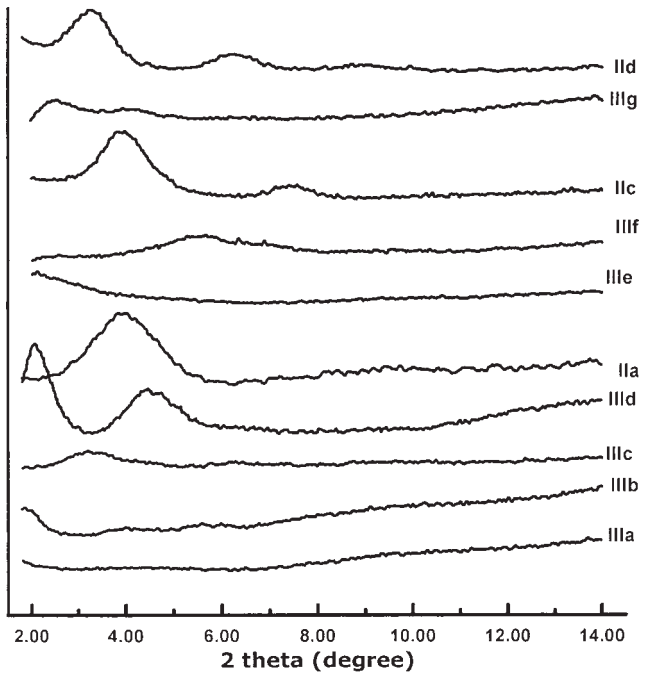

Figure 6 XRD for MMT clay and vinyl monomer–clay $\mathbf{II_a}$, $\mathbf{II_c}$, and grafted PMMA–clay composites $\mathbf{III_{a–g}}$.

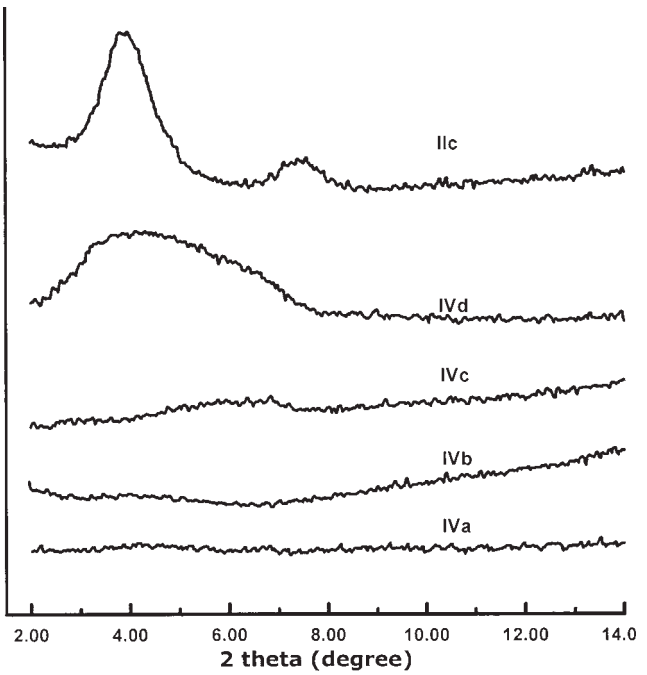

Figure 7 XRD for MMT clay and vinyl monomer–clay $\mathbf{II_c}$ and grafted PHEMA–clay composites $\mathbf{IV_{a–d}}$.

1630 cm^{-1} for $\mathbf{I_b}$, and 1605 cm^{-1} for $\mathbf{I_c}$. The onium salts show characteristic bands corresponding to $—N^{\oplus}R_3$ at 3433 cm^{-1} and $—P^{\oplus}R_3$ at 3414 cm^{-1}. IR spectrum of $\mathbf{I_a}$ shows characteristic bands at 1432, 1157, and 1039 cm^{-1} related to phosphonium salt attached to Ph group. Comparing the bands of $\mathbf{I_a}$ with $\mathbf{II_a}$ showed a shift from 1039 to 916 cm^{-1}, which indicated the interaction of phosphonium salt to metal oxide similar to P—O band. The IR spectrum of $\mathbf{I_b}$ shows characteristic bands at 1457, 1211, and 1098 cm^{-1} corresponding to phosphonium salt attached to butyl group. The band at 1098 cm^{-1} of phosphonium salt was shifted to 911 cm^{-1} in $\mathbf{II_b}$. The broadness of this characteristic band is apparently related to intermolecular interaction. The IR spectrum of $\mathbf{I_c}$ shows characteristic bands at 3600 cm^{-1} for OH group, 2649, 1794 cm^{-1} related to protonated amine group, 1499 cm^{-1} related to ammonium salt itself, and 1348 cm^{-1} related to C—N. The presence of extra peaks for modified clay shows bands around 2920, 2849 cm^{-1} for $—CH_2—$, and around 1831 cm^{-1} for the presence of $—N^{+}H_2—$ group. The characteristic bands of Na-MMT (Fig. 2) show absorption bands at 1030 and 550 cm^{-1} corresponding to the stretching band of Si—O, the deformation band of Si—O—Al, and the Si—O—Si deformation band of MMT. These indicate that organic material stay immobilized inside and on the clay layers. IR spectrum of the grafted polymer–MMT samples (Fig. 2) illustrated that the absorption band of —C=C— disappeared.

The swelling measurements of the vinyl monomer–clay and the grafted polymer–clay composites in different solvents, such as DMF, 1,4-dioxan, acetone, toluene, chloroform, dichloromethane, and water, were listed in Table III as the percentage of sorbed solvent related to the dry weight of the sample. The swelling studies showed that the hydrophilic surface of the clay have been changed to an organophilic nature with treatment by vinyl monomers or grafted polymers. The intercalated vinyl monomers and grafted polymers–clay brought a marked reduction in water

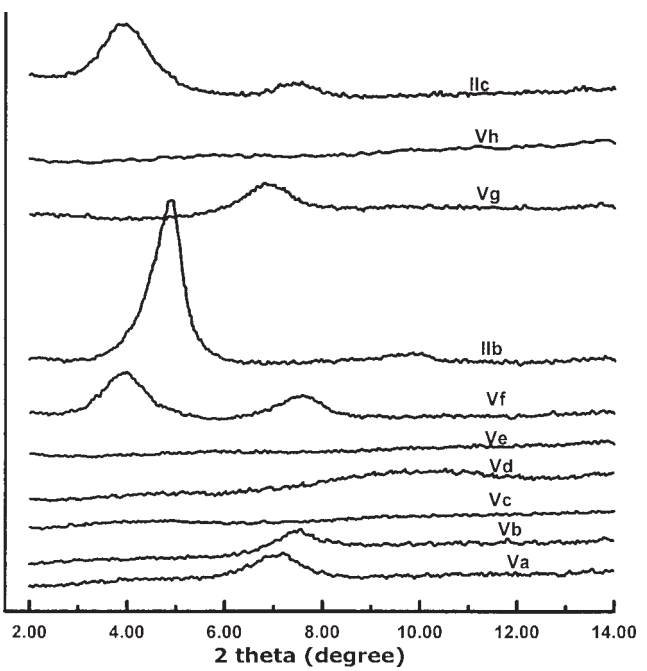

Figure 8 XRD for MMT clay and vinyl monomer–clay $\mathbf{II_b}$, $\mathbf{II_c}$ and grafted P(St-*co*-MA)–clay composites $\mathbf{V_{a–h}}$.

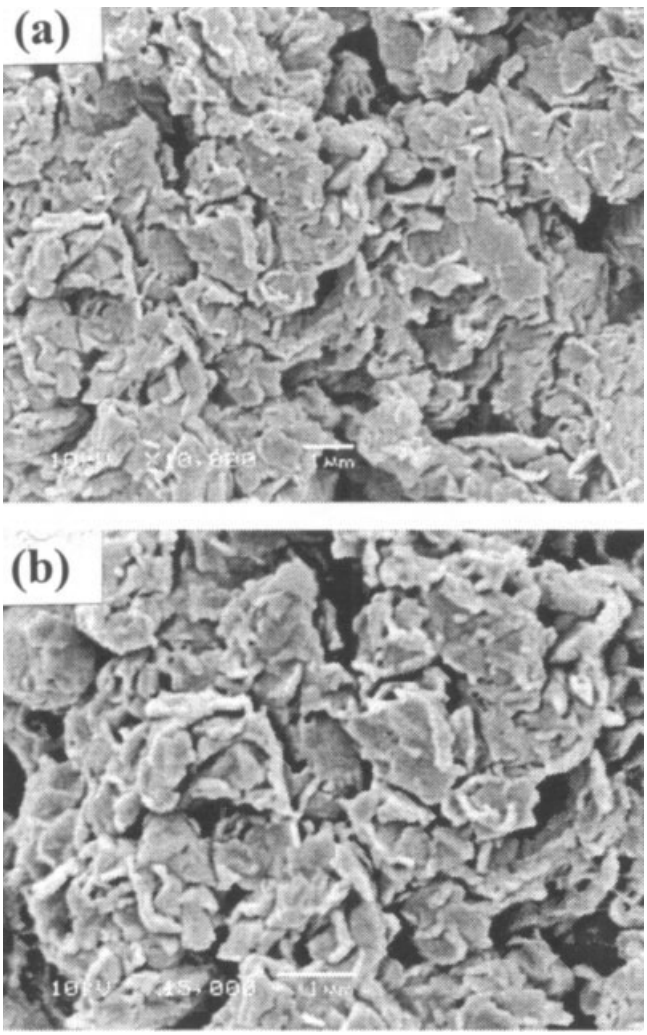

Figure 9 SEM images for the nanocomposite $\mathbf{III_b}$; (a) at magnification 10,000, (b) at magnification 15,000.

affinity of clay, due to the change of an essentially hydrophilic surface to one with organophilic properties. The data in Table III show that the different series of grafted polymers–clay hybrids $\mathbf{III_{a–g}}$, $\mathbf{IV_{a–d}}$, and $\mathbf{V_{a–h}}$ were solvated by a variety of common solvents. The degree of swelling in hydrophobic solvents was decreased as the organoclay ratios increased, since the grafted polymer–clay with small ratios of organoclay ($\mathbf{III_a}$ and $\mathbf{III_b}$) has high swelling than the samples with high ratios ($\mathbf{III_c}$ and $\mathbf{III_d}$). In another way, the samples prepared by bulk polymerization ($\mathbf{III_e}$ and $\mathbf{III_f}$) show less swelling than the samples prepared by solution polymerization ($\mathbf{III_b}$ and $\mathbf{III_c}$). This may be due to the increase of the polymer chain contents. Also, the nature and structure of the grafted polymers onto the clay are significant factors affecting the swelling degree. The polymers having groups capable of formation of H-bond interaction with MMT shows higher swelling, since the swelling order is PMMA > PHEMA > P(St-*co*-MA). Nature of the solvents plays as an important factor affecting the swelling degrees, since the aprotic solvent show higher swelling degrees than protic solvent.

Thermal properties of the vinyl monomer–clay and the polymer–clay nanocomposites were investigated by using the TGA analysis. The data are listed in Table IV and thermograms illustrated in Figures 3 and 4. The data includes the onset temperature for the starting the degradation and the temperatures at which 5% ($T_{0.05}$) and 10% ($T_{0.1}$) degradations are occurred. Also, Table IV shows the temperatures at which 50% degradation ($T_{0.5}$), the mid-point of the degradation process, the thermal stability for the sample under measurements, and the fraction of materials, which does not volatilize at 800°C, denoted as char.

TGA data in Table IV and Figure 3 show the onset temperature of 5% and/or 10% degradation, which is affected by the quaternary onium groups, attached to the MMT clay. It was found that the degradation temperature is higher for materials attached through phosphonium group compared with materials attached through ammonium groups. This may be due to the degradation of organically modified clay, occurred by

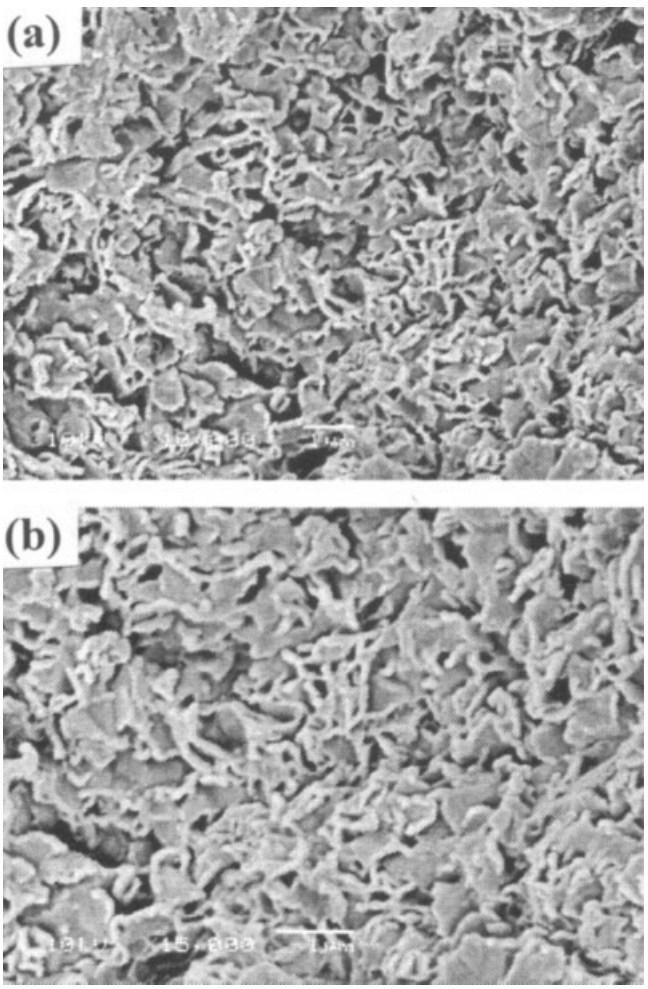

Figure 10 SEM images for the nanocomposite $\mathbf{III_c}$; (a) at magnification 10,000, (b) at magnification 15,000.

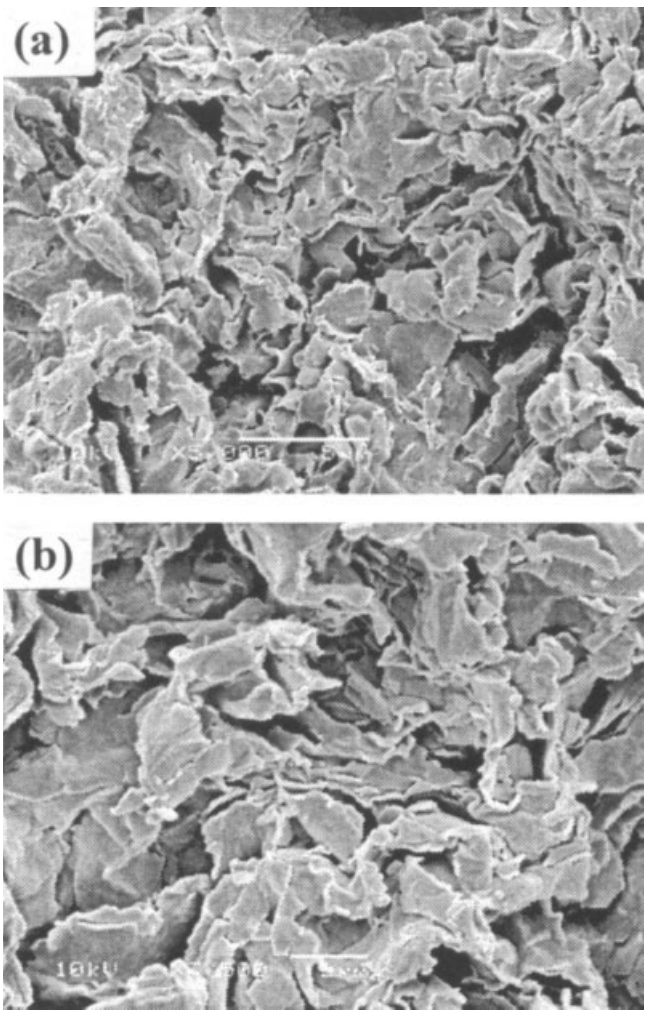

Figure 11 SEM images for the nanocomposite $\mathbf{V_d}$; (a) at magnification 5000, (b) at magnification 7500.

a Hofmann elimination reaction producing olefin and amine, leaving a proton occupying the cationic position on the clay (Scheme 3).[22] Also, it was found that the amount of char was increased with increasing the clay contents. This enhancement may be due to presence of aromatic ring structure and high stability of phosphonium cation. The disubstituted amine surfactant attached to the clay $\mathbf{II_d}$ shows lower thermal stability than primary amine surfactant attached to the clay $\mathbf{II_c}$, which may be attributed to the presence of H-bond between MMT and $—^{+}NH_2—$.

The thermal stabilities of PMMA–clay and PHEMA–clay intercalates are based on the chemical structure and restricted thermal motion of polymer chains in the silicate interlayers. Figure 3 and Table IV show that the onset degradation temperatures of polymer–clay samples are decreased with increasing the amount of clay in the samples $\mathbf{III_b}$ and $\mathbf{III_c}$, which may be attributed to the decreased exfoliation ratio of clay in the polymer matrix. Figure 3 shows the thermograms of the polymer–clay, which consist of more

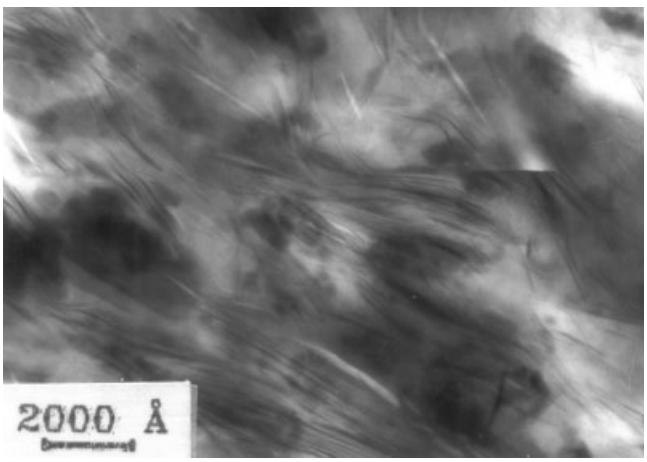

Figure 12 TEM images for the nanocomposite $\mathbf{III_e}$.

than one step. The magnitude of the degradation steps changes from sample to another depending on the nature of the polymer–clay composite. Also, Figure 3 illustrates the degradation of PHEMA in the sample $\mathbf{IV_b}$, which occurs in three steps. The first step range from 190 to 310°C, due to the degradation of ammonium salt through Hoffman elimination with the ratio $\sim$ 8%. The second step is related to the degradation of physical attached polymers on the clay surface, which occur in the temperature range 310–395°C and involve $\sim$ 31% of the degradation process. The third step ranging from 395 to 465°C is due to the degradation of chemically attached polymer through vinyl-cation and involves $\sim$ 58% of the degradation process.

Figure 4 shows TGA thermograms of P(St-*co*-MA)-MMT composites, in which the decomposition of these materials occurred in one step or more. The thermogram of composite $\mathbf{V_b}$ shows the degradation in two steps in the temperature ranges 120–335°C and 345–455°C. These may be attributed to the degradation of the chemically and physically grafted polymers, which are either interacted inside or adsorbed outside

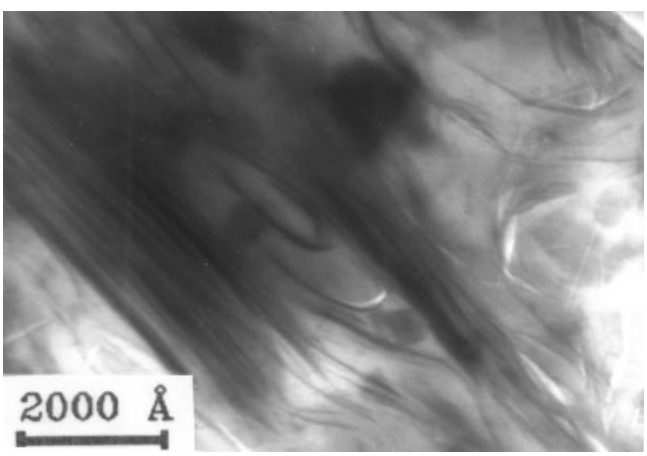

Figure 13 TEM images for the nanocomposite $\mathbf{V_d}$.

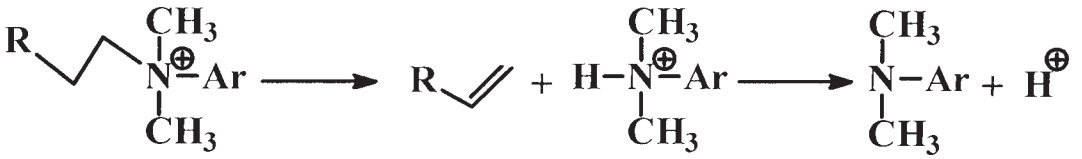

Scheme 3 Degradation of ammonium salts according to Hofmann elimination reaction.

clay galleries. Whereas the sample $\mathbf{V_h}$ shows decomposition that occurs in three steps in the temperature ranges 100–265°C, 265–380°C, and 380–460°C. This may be attributed to the degradation of the surfactant on the clay surface and the chemically and physically grafted polymers. The thermograms of samples $\mathbf{V_d}$ and $\mathbf{V_e}$ show one degradation step in the temperature range 288–640°C and 171–609°C, respectively. The difference between the two samples may be due to the use of different solvent during polymerization, since the high swelling of vinyl monomer–clay of $\mathbf{V_e}$ in MeCN increases amount of P(St-*co*-MA) and leads to higher *d*-spacing between clay interlayers and hence decreases the degradation temperature range when compared with the use of toluene in preparation of $\mathbf{V_d}$.

From the definition of the nanocomposite, the particle size of the disperse phase is lower than 10^2 nm at least in one dimension.[23] When the inorganic MMT is treated with a vinyl-organic ammonium or phosphonium salts, it becomes hydrophobic and the interlayer galleries are also enlarged. During the polymerization, the small monomer molecules can easily enter the galleries and grow up to form polymer together with the attached vinyl groups. According to the intercalative polymerization mechanism, the interlayer spacing of MMT should be enlarged and intercalated or exfoliated by formation of homo and grafted polymer chains attached to MMT. The evidence of the proposed mechanism is provided by XRD, SEM, and TEM analyses. The formation of a delaminated structure usually results in the complete loss of registry between the clay galleries where the intercalated structure results from registry between clay galleries.

The XRD patterns of vinyl monomer-MMT (Fig. 5) show that the *d*-spacing of the intercalated monomers into MMT is affected by the molecular mass of the monomer. The *d*-spacing was increased from 12.0 Å ($2\theta = 7.2°$) for Na-MMT clay to 23.12 Å ($2\theta = 3.82°$) for $\mathbf{II_a}$, 18.29 Å ($2\theta = 4.83°$) for $\mathbf{II_b}$, 23.0 Å ($2\theta = 3.83°$) for $\mathbf{II_c}$, and 33.6, 18.48 Å ($2\theta = 2.63°, 4.78°$) for $\mathbf{II_d}$, indicating that the cations were intercalated into the silicate layers of MMT. The results revealed that the increases in *d*-spacing are in the order of $\mathbf{II_d} > \mathbf{II_c} \approx \mathbf{II_a} > \mathbf{II_b}$, which coincide with the order of the molecular weight of the monomers $\mathbf{I_d}$, $\mathbf{I_c}$, $\mathbf{I_a}$, and $\mathbf{I_b}$ (450, 422, 414, and 354, respectively). The small intense and broad peak at $2\theta = 7°$ for the sample $\mathbf{II_c}$ may arise from the incomplete exchange process of sodium ion in MMT by ammonium ion of vinyl monomer modifier, due to the incomplete swelling during the preparation. Also, there are two peaks for the vinyl monomer–clay $\mathbf{II_d}$, the first peak found at $2\theta = 2.63°$ corresponding to the solid-like packing of the intercalated $\mathbf{I_d}$, whereas the second peak found at $2\theta = 4.78°$ corresponding to the tilted molecule liquid-like packing. Also, this may be due to the lack interlayers symmetrical arrangement of modified clay.[24]

The XRD results for grafted polymer–MMT $\mathbf{III_{a–f}}$, $\mathbf{IV_{a–d}}$, and $\mathbf{V_{a–j}}$ are shown in Figures 6–8. Figure 6 shows two series of XRD patterns for the grafted PMMA-MMT composites with vinyl monomer-MMT $\mathbf{II_a}$ and $\mathbf{II_c}$. The diffraction peak corresponding to d_{001} was disappeared in the composite sample $\mathbf{III_a}$ containing 1 wt % organoclay $\mathbf{II_a}$. This is an indication to the formation of exfoliated nanocomposites in which the MMT is homogenously dispersed in the PMMA matrix. In another way, a weak and broad peak at $2\theta = 2.2$ and 2.47°–3.67° for the samples $\mathbf{III_b}$ and $\mathbf{III_c}$ containing 5 and 10 wt % of $\mathbf{II_a}$ was found. This can be explained by formation of partially exfoliated/intercalated nanocomposites. However, Wilkie and Su reported a similar result in the preparation of PMMA–clay hybrids, with an intercalated morphology obtained at 5% clay.[25] Also, a strong peak was observed at $2\theta = 4.4°$ for the sample $\mathbf{III_d}$ containing 25 wt % of $\mathbf{II_a}$, which results from collapsed intercalated layer and the enhanced ordering in the MMT layers of the composite. The bulk polymerization of MMA with vinyl monomer-MMT $\mathbf{II_c}$ gives exfoliated PMMA–clay nanocomposites $\mathbf{III_e}$, since there is no beak corresponding to d_{001} (Fig. 6). Figure 6 shows also a broad peak at $2\theta = 4.7°$–6.1° for the intercalated P(MMA)–clay nanocomposite $\mathbf{III_f}$, which can be explained as the insufficient monomer present within the clay layers to reach the fully exfoliated structure.

Figure 7 shows a series of XRD patterns for PHEMA-MMT $\mathbf{IV_{a–d}}$ prepared from vinyl monomer-MMT $\mathbf{II_c}$. No peaks were detected for the samples $\mathbf{IV_{a–c}}$, which indicate the formation of an exfoliated polymer–clay nanocomposites. However, the sample $\mathbf{IV_d}$ has a broad peak at $2\theta = 2.5°$–7.1°, which can be attributed to a partial exfoliated/intercalated structure due to increasing the contents of MMT.

Figure 8 shows two series of XRD patterns for the P(ST-*co*-MA)-MMT composites with vinyl monomer-MMT $\mathbf{II_{b,c}}$. In Figure 8, no peaks were observed for the

samples $\mathbf{V_{c-e}}$ containing 5 and 10 wt % vinyl-MMT. This indicates the formation of exfoliated nanocomposites. However, in case of the samples $\mathbf{V_{a,b}}$ the diffraction peaks below $2\theta = 4.83^\circ$ disappeared, but a new peak was observed at $2\theta = 7.1^\circ$ corresponding to the peak on net Na^{+-}O-MMT results from degradation of onium salt.[22] Also, a strong peak at $2\theta = 3.8^\circ$ for the sample $\mathbf{V_f}$ was found, which is an indication for the formation of intercalated nanocomposite.

More evidence for the formation of the nanocomposites is provided by SEM and TEM. The examination of the surface of the deposited samples was followed with SEM. The micrographs indicate that the polymers were intercalated in the interlayer of MMT in a homogenous manner to produce new polymer–MMT composite materials. The micrograph does not show the MMT particles on the micron level. Figures 9–11 show micrographs of the surface at different magnifications (5000–15,000) for the samples $\mathbf{III_b}$, $\mathbf{III_c}$, and $\mathbf{V_d}$. The absence of MMT particles indicates that the agglomerate did not reveal the inorganic domains. The particle size of MMT (0.1–10 μm) is not visible due to well adherence to the polymer and it is below the magnification of SEM. This indicates that the mineral domains are submicron and homogenously dispersed in the polymer matrix. It indicates also that the polymer was intercalated in the interlayer of MMT in a homogenous manner to produce new polymer–MMT nanocomposite materials.

The transmission electron micrographs of a thin film for samples $\mathbf{III_e}$ and $\mathbf{V_d}$ are illustrated in Figures 12 and 13. The images of the individual silicate layers appear as dark lines and indicate that the separation between the dispersed plates is irregular with a good particle–matrix adhesion in the range of 150–300 Å.

CONCLUSIONS

Series of several grafted polymer–organoclay nanocomposites have been prepared via *in situ* polymerization of different monomers onto vinyl monomer-MMT. The preparation was carried out by modification of the MMT with different vinyl monomer salts, followed by the free-radical polymerization of MMA, HEMA, or St-*co*-MA monomers with different ratios of vinyl monomer-MMT. The intercalation of vinyl monomer-cations within the clay interlayers was verified by IR spectra. The thermal properties were determined from the TGA, which shows higher thermal stability for polymer–MMT nanocomposites than polymers. The TGA showed the formation of polymer–organoclay nanocomposites through the interaction between phosphonium moieties of the modified MMT and the polymer and showed also higher thermal stability for polymer–organoclay nanocomposites than those with ammonium moieties. The swelling measurements in different organic solvents showed that the swelling degree in hydrophobic solvents increases as clay ratio decrease. The XRD analysis illustrates that the nanocomposites were exfoliated at up to 25 wt % of organoclay contents. The SEM shows a complete dispersion of polymers into clay interlayers. Also, TEM shows formation of nanosize particles ranged 150–300 Å in the images.

References

1. Mohanty, A. K.; Misra, M.; Drzal, L. T. Compos Interface 2001, 8, 313.
2. Oya, A. In Polymer Clay Nanocomposites; Pinnavaia, T. J., Beall, G. W., Eds.; London: Wiley, 2000; pp 151–172.
3. Alexandre, M.; Dubois, P. Mater Sci Eng R 2000, 28, 1.
4. Shi, H.; Lan, T.; Pinnavaia, T. Chem Mater 1996, 8, 1584.
5. Messersmith, P. B.; Giannelis, E. P. Chem Mater 1994, 6, 1719.
6. Lan, T.; Pinnavaia, T. Chem Mater 1994, 6, 2216.
7. Lee, D. C.; Jiang, L. W. J Appl Polym Sci 1998, 68, 1997.
8. Noh, M. W.; Lee, D. C. Polym Bull 1999, 42, 619.
9. Zhu, J.; Wilkie, C. A. Polym Int 2000, 49, 1158.
10. Doh, J. G.; Cho, I. Polym Bull 1998, 41, 511.
11. Vaia, R. A.; Giannelis, E. P. Macromolecules 1997, 30, 8000.
12. Liu, L. M.; Qi, Z. N.; Zhu, X. G. J Appl Polym Sci 1999, 71, 1133.
13. Carrado, K. A.; Xu, L. Q. Chem Mater 1998, 10, 1440.
14. Okamoto, M.; Morita, S.; Kim, Y. H.; Kotaka, T.; Tateyama, H. Polymer 2001, 42, 1201.
15. Wang, D.; Zhu, J.; Yao, Q.; Wilkie, C. A Chem Mater 2002, 14, 3837.
16. Hwu, J. M.; Jiang, G. J.; Gao, Z. M.; Pan, W. P. J Appl Polym Sci 2002, 83, 1702.
17. Zhu, J.; Start, P.; Mauritz, A. K.; Wilkie, C. A. Polym Degrad Stab 2002, 77, 253.
18. Akelah, A.; Rehab, A.; Agag, T.; Betiha, M. J Appl Polym Sci 2007, 103, 3739.
19. Akelah, A.; Moet, A. J Mater Sci 1993, 31, 3589.
20. Kawasumi, M.; Hasegawa, N.; Kato, M.; Usuki, A.; Okada, A. Macromolecules 1997, 30, 6333.
21. Billmeyer, F. W. Textbook of Polymer Science, 3rd ed; New York: Wiley Interscience, 1984.
22. Xie, W.; Gao, Z.; Pan, W. P.; Vaia, R.; Hunter, D.; Singh, A. Polym Mater Sci Eng 2000, 83, 284.
23. Calvert, P. Nature (London) 1996, 383, 300.
24. Vaia, R. A.; Teukolsky, R. K.; Giannelis, E. P. Chem Mater 1994, 6, 1017.
25. Su, S.; Wilkie, C. A. J Polym Sci Part A: Polym Chem 2003, 41, 1124.